GSA DATA REPOSITORY 2019038

Appendix DR1. Description of methods, Tables DR1-DR2, Figures DR1-DR3

Sequestration and subduction of deep-sea carbonate in the global ocean since the Early Cretaceous

Adriana Dutkiewicz, R. Dietmar Müller, John Cannon, Sioned Vaughan, Sabin Zahirovic

*corresponding author: adriana.dutkiewicz@sydney.edu.au

METHODS

Carbonate sedimentation rates

Coccolithophores and associated nannoplankton are the largest contributors of carbonate to the deep sea (Baumann et al., 2005; Berger, 2011), first appearing in the geological record in the Late Triassic (~220 Ma) (Bown et al., 2004). Despite rapid diversification, their production was low throughout most of the Jurassic and restricted to shelf seas (Hay, 2004; Roth, 1986), shifting to the open ocean in the late Jurassic (~ 150 Ma) in a major event that changed the global carbonate system (Roth, 1989). Planktonic foraminifera that are also a significant component of pelagic carbonates first appear in the Middle Jurassic (~ 170 Ma) (Knoll, 2003) but only became major producers of carbonate sediment in the Neogene (from ~ 23 Ma) (Roth, 1986).

Sedimentation rates for pelagic carbonates deposited during the Mesozoic are difficult to constrain because there are few deep-sea drill sites that penetrate to basement, have good core recovery, and have reliable and complete age-depth relationships (Fig. 2, Table DR1). For our preferred model (Model 1) that results in the best comparison with observed carbonate sediment thicknesses from deep-sea drill sites, we assume that deep-sea pelagic carbonate sedimentation rate prior to 170 Ma was zero. From 170 Ma to 152 Ma we estimate that the sedimentation rate was only 0.2 cm/ky, increasing to 0.5 cm/ky between 152 Ma and 144 Ma based on decompacting the values from Bornemann et al. (Bornemann et al., 2003). From 144 Ma to present-day we assume a constant sedimentation rate of 1.8 cm/ky based on a median calculated from 160 deep-sea surface carbonate sediments containing > 50% CaCO3 (see Fig. 2 in Dutkiewicz et al. (2017)). This is consistent with a global average of 1–3 cm/ky for calcareous oozes (Kennett, 1982) and captures temporal and spatial variations evident in deep-sea drill sites removed from continents and upwelling regions during their lifetime (Davies and Worsley, 1981). We run additional models using alternative sedimentation rates that provide minimum (Model 2, Table DR1) and maximum (Model 3, Table DR1) constraints on our model. We also use long-term sedimentation rates from Opdyke and Wilkinson (1988) based on Deep Sea Drilling project data from Whitman and Davies (Whitman and Davies, 1979);

however, these sedimentations rates are very low and result in a poor agreement with observed thicknesses (Fig. DR1).

Table DR1. Sedimentation rate models. Model 1 results in the most favourable comparison with present-day carbonate thicknesses (see Fig. 2 and Fig. DR1).

Time (Ma)	Sedimentation rate (cm/ky)
Model 1 (preferred)	
Prior to 170	0
170–152	0.2
152–144	0.5
144–0	1.8
Model 2 (minimum)	
Prior to 170	0
170–152	0.2
152–144	0.5
144–0	1.6
Model 3 (maximum)	
Prior to 170	0
170–152	0.2
152–144	0.5
144–0	2.0
Model 4 (from Opdyke and Wilkinson *(34)*)	
180–170	0
170–60.5	0.2
60.5–35.2	0.3
35.2–27.7	0.5
27.7–18.9	0.4
18.9–12.1	0.5
12.1–9.6	0.6
9.6–6	0.7
6–4.5	0.8
4.5–3.1	0.9
3.1–2.4	1.0
2.4–0	1.1

Carbonate Compensation depth (CCD) and its uncertainties

The process of seafloor spreading slowly moves calcareous sediment and the underlying young ocean crust at mid-ocean ridges to deeper regions of the ocean where sediments overlying older carbonate-rich deposits are carbonate-free, having been deposited on ageing ocean crust at greater depths below the CCD.

In addition to the global CCD curve of Boss and Wilkinson (1991), we ran all the sedimentation rate models using the global CCD curve of Opdyke and Wilkinson (1988), which is based on combined CCDs from Van Andel (1975) and Broecker and Peng (1982). Sensitivity analysis shows that the combination of the Boss and Wilkinson (1991) global CCD and Model 1 sedimentation rates results in the best overall agreement with observed carbonate sediment thickness (Fig. 2, Fig. DR1).

The uncertainties in CCD depth estimates include uncertainties in reconstructed basement depth, which can be summarized as any sediment-unloaded basement depth deviations from an ideal age-depth relationship. A widely used age-depth relationship is the plate model by Stein and Stein (1992). Müller et al. (2008) used this model, together with their oceanic crustal ages and a global sediment thicknesses to compute a residual basement depth grid. This grid outlines regional deviations from the expected basement depth based on an age-depth relationship that assumes that all mid-ocean ridge crests have the same initial depth and the same crustal thickness, and that all mid-ocean ridge flanks follow the same tectonic subsidence curve. The median residual basement depth based on this model is 150 m, providing a global estimate of the uncertainty in reconstructing basement depth. Additional uncertainties in reconstructing CCD depth include errors in decompacting sediments, uncertainties introduced by unconformities and in identifying the CCD based on the measured sedimentary carbonate fraction. Van Andel (1975) estimated all uncertainties, other than those related to basement depth, to average ± 150 m. We adopt this estimate, yielding a total uncertainty of ± 300 m in CCD depth estimates. The uncertainty is incorporated into our sensitivity analysis (Fig. DR1H and DR1I) and error envelopes (Fig. 1).

Lysocline

Our model considers that dissolution of carbonate occurs ~ 300 m above the CCD with carbonate content of sediment decreasing from near 100% at the lysocline (Milliman, 1993), a sediment property where dissolution becomes noticeable, to 0% at the CCD (Ridgwell and Zeebe, 2005).

Paleobathymetry calculation

We follow the method described in Müller et al. (2008) to construct oceanic paleo-depth maps by converting oceanic paleo-age from Müller et al. (2016) to basement depth, and for including the elevation of major large igneous provinces (LIPs). Sediment thickness through time, including its isostatic effect, is added by considering its dependence on age and proximity to passive continental margins through time (Dutkiewicz et al., 2017). These paleo-bathymetry maps form the basis for computing intersections of the carbonate compensation depth with the seafloor.

Carbonate thickness calculation

At each 1 My time step from 0 to 120 Ma, a decompacted and compacted carbonate sediment thickness grid with 0.5° resolution is generated. Additionally, a mask grid is generated at each time step that represents where on the current seafloor carbonate is currently (at that time step) being deposited, and hence does not include the deposition history over the lifetime of the current ocean floor. A uniform distribution of points in latitude and longitude is generated for each grid at each time. At each grid point we

sample input bathymetry, crustal age and mean distance to passive margins using input data grids representing those respective quantities at a specific time on the ocean floor. These input data are used at each grid point to model the bathymetry of a parcel of ocean floor over its lifetime. This allows us to trace the bathymetry history of the parcel of ocean floor (at that grid point) and compare it with the CCD, which also varies over the ocean parcel's history. Note that the carbonate sedimentation rate is only non-zero for those time intervals when the parcel's bathymetry is above the CCD. The carbonate sedimentation rate is modelled to vary linearly with depth through the lysocline from the maximum rate associated with the bathymetry at the initiation of the parcel (at the mid-ocean ridge when its age is zero) to zero sedimentation rate at the CCD. The maximum sedimentation rate curve is sampled at each time in the history of a single parcel, rather than sampled only at the time when the parcel is at the mid-ocean ridge.

The varying carbonate sedimentation rate over the ocean parcel's lifetime is then accumulated over these time intervals (when modelled bathymetry is above CCD) to obtain the total decompacted carbonate sediment thickness, which can be used as a measure of total carbonate content at the current time. A compacted carbonate thickness is also calculated. For this we assume an average sediment density of 2647 kg/m^3, a porosity of 0.66, and decay constant of 1333 m (Kominz et al., 2011) to provide an indication of what the total sediment thickness would be if only carbonate were deposited. The bathymetry over the ocean parcel's lifetime is modelled as tectonic subsidence (sediment-free depth) plus an isostatically compensated total compacted sediment thickness. The seafloor subsidence is obtained by converting ocean floor age to depth using the GDH1 model (Stein and Stein, 1992). The total compacted sediment thickness is predicted using a bicubic polynomial of the ocean parcel's age and mean distance to passive margins over the parcel's lifetime (Dutkiewicz et al., 2017). A constant offset is applied to the bathymetry model to ensure that it matches the known bathymetry (obtained from the input grid) at the current age of the parcel of ocean crust.

Subducted carbonate calculation

This calculation is performed using a published workflow based on the pyGPlates python library (www.gplates.org and https://github.com/EarthByte/PlateTectonicTools) and is outlined in (Müller and Dutkiewicz, 2018).

Table DR2. DSDP and ODP data for sites drilled to oceanic basement. Crustal ages obtained from the present-day age grid of Müller et al. (2016). Water depth is obtained from the ETOPO1 model of Amante and Eakins (2009). Depth to basement and lithology overlying basement from DSDP and ODP initial reports and proceedings volumes. Observed total carbonate thicknesses (100% carbonate) calculated for each site are based on stratigraphy and unit thickness from DSDP and ODP initial reports and proceedings volumes, and $CaCO_3$ contents from DSDP and ODP initial reports and proceedings volumes obtained via the National Centres for Environmental Information (NCEI) at the National Oceanic and Atmospheric Administration (NOAA) (https://www.ngdc.noaa.gov/mgg/fliers/00mgg03.html and https://www.ngdc.noaa.gov/mgg/geology/data/joides_resolution/odp_2001_cdrom/), IODP LIMS (LORE) Reports (http://iodp.tamu.edu/LORE/) and PANGAEA® Data Publisher (https://www.pangaea.de/). The model results are based on the sedimentation rate model 1 (Table DR1) and global CCD from (Boss and Wilkinson, 1991).

Site	Long. (°)	Lat. (°)	Ocean region	Crustal age (My)	Water Depth (m)	Depth to basement (m)	Lithology overlying basement	Total compacted carbonate thickness (m)		
								Observed	Modelled	Difference
332	-33.64	36.88	North Atlantic	3.1	1729	105	foram-bearing nannofossil ooze	96.5	25.8	70.7
396	-43.52	22.99	North Atlantic	13.6	4452	125	calcareous clay interbedded with marly nannofossil ooze	101.8	84.2	17.6
9	-59.20	32.77	North Atlantic	103.7	5012	834.5	zeolitic clay	20.3	21.5	-1.2
137	-27.06	25.93	North Atlantic	105.7	5389	397	nannofossil marl ooze	69.7	24.8	44.9
417	-68.04	25.11	North Atlantic	119.9	5464	343	clayey nannofossil chalk	16.9	40.4	-23.5
543	-58.65	15.71	North Atlantic	——	5560	411	calcareous ferruginous claystone	1.2	23.8	-22.6
15	-17.98	-30.89	South Atlantic	19.6	3933	140.6	nannofossil ooze	108	121.9	-13.9
19	-23.68	-28.53	South Atlantic	46.3	4583	140.9	nannofossil chalk ooze with hematite	78	83.6	-5.6
894	-101.53	2.30	North Pacific	0.9	4473	9.3	calcareous ooze and foram sand	7.5	4.8	2.7
856	-128.68	48.44	North Pacific	1.1	2473	115.7	hemipelagic and turbiditic sediments	3	5.0	-2.0
485	-107.90	22.75	North Pacific	1.2	3016	153.5	silty clay	9.1	12.6	-3.5
1256	-91.93	6.74	North Pacific	15.3	3627	250.7	nannofossil ooze with some clay	132.5	93.1	39.4
1224	-141.98	27.89	North Pacific	46.3	4978	28	clay	0	71.3	-71.3
1215	-147.93	26.03	North Pacific	58.4	5409	69.2	metalliferous sediment	32.8	39.4	-6.6
192	164.71	53.01	North	104.8	2997	1044	chalk and	36.2	20.7	15.5

			Pacific				calcerous claystone			
164	-161.52	13.20	North Pacific	109.2	5464	256	cherty claystone	1.3	30.4	-29.1
464	173.89	39.86	North Pacific	114.4	4663	307.6	chert limestone	55.2	31.1	24.0
66	-166.12	2.39	North Pacific	121.7	5331	193	radiolarian clay	0.6	15.2	-14.6
303	154.45	40.81	North Pacific	126.1	5637	284.8	cherty nannofossil ooze	10.2	24.9	-14.7
1179	159.96	41.08	North Pacific	128.0	5578	377.2	chert within unknown lithology	3	31.1	-28.1
166	-175.08	3.76	North Pacific	128.1	4946	307	nannofossil marlstone	25.7	31.6	-5.8
304	155.07	39.34	North Pacific	128.9	5662	334 .5	nanno ooze and chert	17.0	34.0	-17.0
1149	143.35	31.34	North Pacific	133.0	5818	407.8	radiolarian chert and radiolarian nanno marl	63.1	46.5	16.6
307	161.01	28.59	North Pacific	146.4	5661	298	nannofossil claystone	28.2	8.6	19.6
169	173.55	10.67	North Pacific	151.0	5361	233	cherty nannofossil chalk	13.2	6.3	6.9
801	156.36	18.64	North Pacific	171.0	5675	461.6	radiolarian claystone	7.7	2.5	5.2
838	-176.89	-20.83	South Pacific	2.5	2315	153.8	basaltic gravel	26.7	16.3	10.4
595	-165.53	-23.82	South Pacific	93.8	5633	69.8	cherty claystone	0	6.3	-6.3
250	39.37	-33.46	Indian	93.1	5118	725.3	detrital clay	28.9	10.3	18.5
256	100.78	-23.46	Indian	110.4	5205	251	detrital clay	0.0	34.2	-34.2
257	108.35	-30.99	Indian	115.9	5257	262	detrital clay	8.0	52.0	-44.1
261	117.89	-12.95	Indian	150.9	5654	532.5	nannofossil claystone	86.1	99.2	-13.1
265	109.95	-53.54	Indian	13.9	3646	444.5	clay and diatom-bearing nannofossil ooze	87.5	85.3	2.2
266	110.11	-56.40	Indian	22.7	4266	370.3	nannofossil claystone	108.2	139.5	-31.3
213	93.90	-10.21	Indian	57.0	5584	154	zeolitic clay	8.3	41.9	-33.6
240	50.05	-3.49	Indian	65.1	5076	190	nannofossil ooze, silty clay, sandy silt, and sand	27.6	48.5	-20.9
239	51.68	-21.30	Philippine Sea	70.4	4968	320	nannofossil claystone	90.3	63.5	26.8
323	-98.00	-63.68	Southern	75.2	4992	701	zeolitic clay	6.7	31.4	-24.7

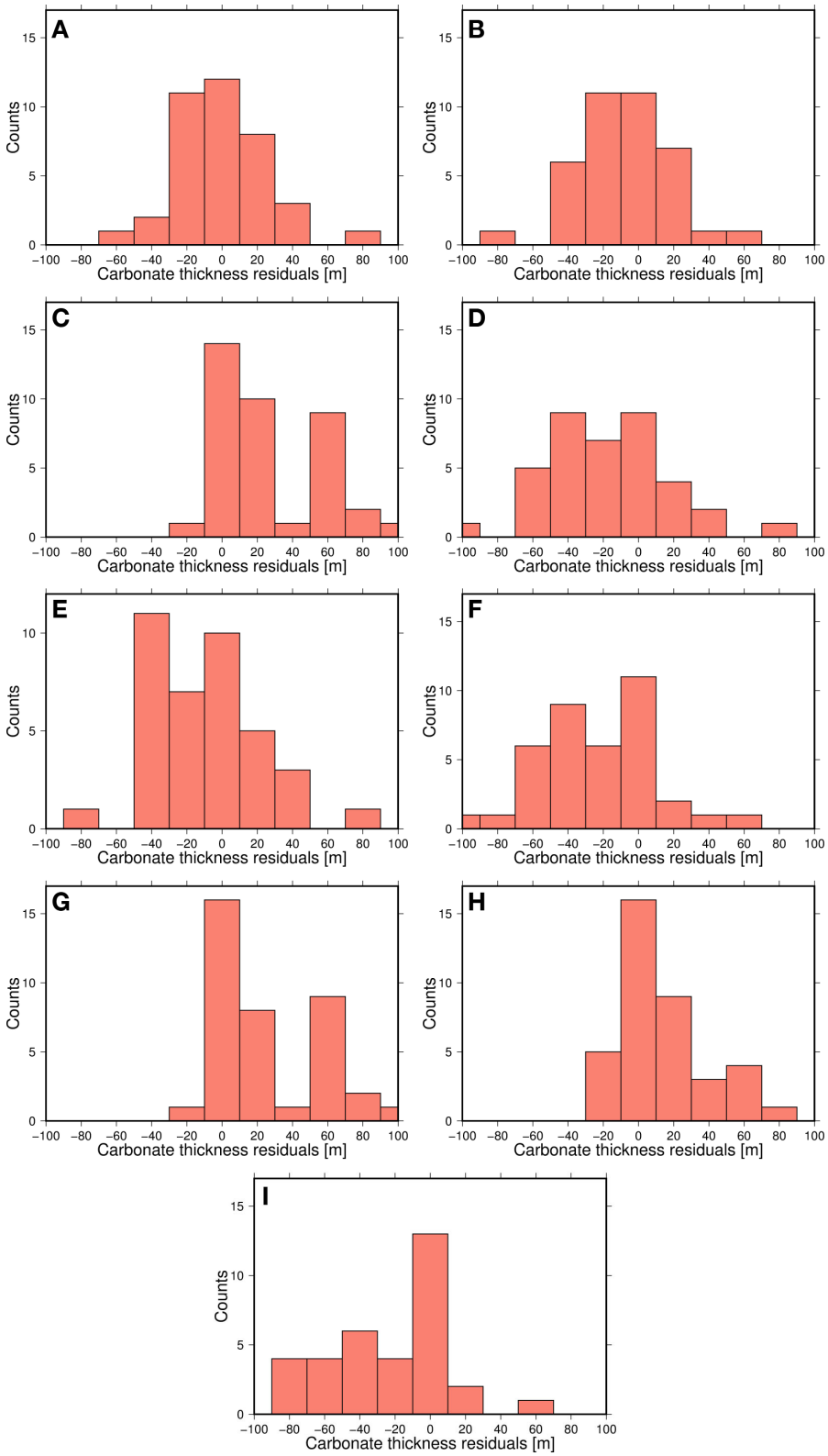

Figure DR1. Distribution of carbonate thickness residuals showing the difference between various modelled thicknesses and observed carbonate thickness from the Deep Sea Drilling Project (DSDP) and Ocean Drilling Program (ODP) (see Table DR2 and Fig.

2). Sedimentation rate models are shown in Table DR1. Note that the residuals based on our preferred best-fit model using sedimentation rate model 1 and the global CCD from Boss and Wilkinson (1991) are shown in Fig. 2. **(A)** Global CCD from Boss and Wilkinson (1991) and sedimentation rate model 2. **(B)** Global CCD from Boss and Wilkinson (1991) and sedimentation rate model 3. **(C)** Global CCD from Boss and Wilkinson (1991) and sedimentation rate model 4. **(D)** Global CCD from Opdyke and Wilkinson (1988) and sedimentation rate model 1. **(E)** Global CCD from Opdyke and Wilkinson (1988) and sedimentation rate model 2. **(F)** Global CCD from Opdyke and Wilkinson (1988) and sedimentation rate model 3. **(G)** Global CCD from Opdyke and Wilkinson (1988) and sedimentation rate model 4. **(H)** Global CCD from Boss and Wilkinson (1991) with -300 m error and sedimentation rate model 2. **(I)** Global CCD from Boss and Wilkinson (1991) with +300 m error and sedimentation rate model 3.

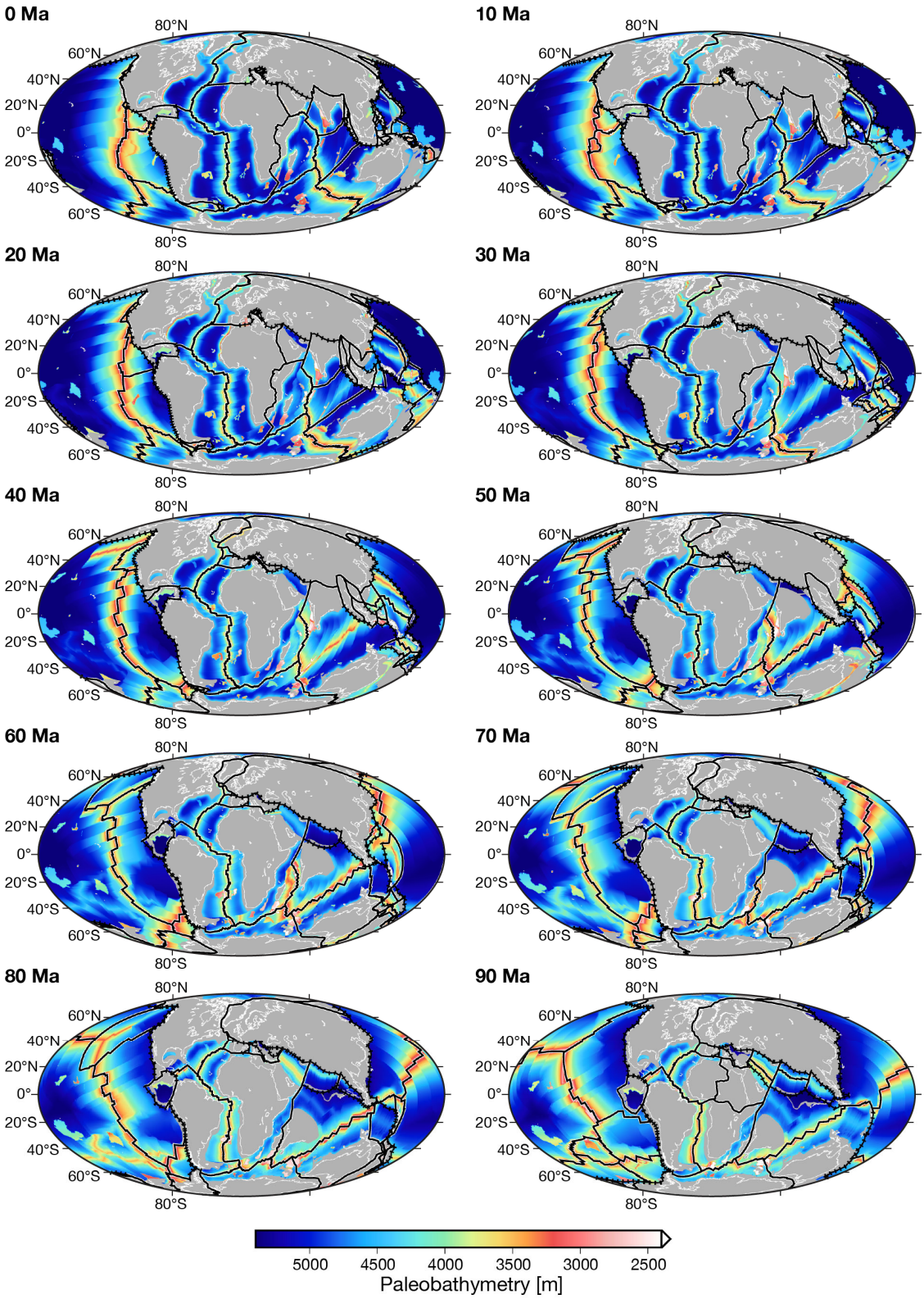

Figure DR2. Plaeobathymetry shown at 10 Myr intervals. Subduction zones (black hatched lines), other plate boundaries (black lines with white outlines), and paleo-coastlines (white outlines) on continents (gray) are shown. Mollweide projection.

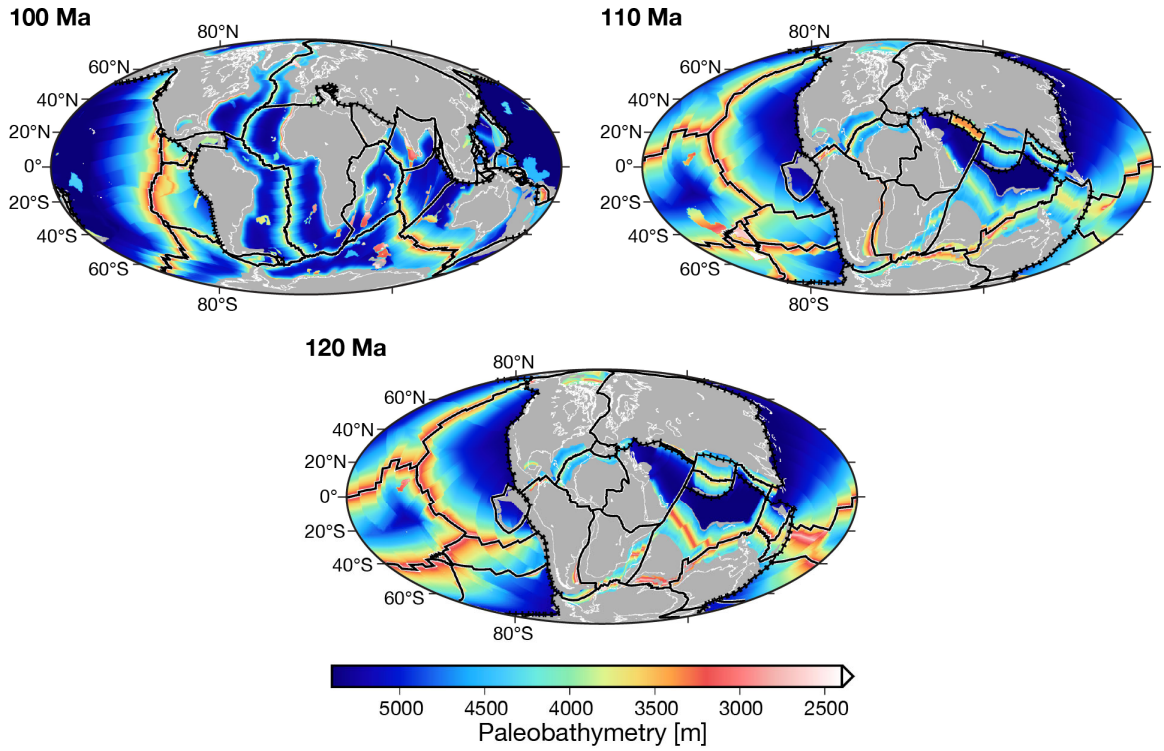

Figure DR2 cont. Paleobathymetry shown at 10 Myr intervals. Subduction zones (black hatched lines), other plate boundaries (black lines with white outlines), and paleo-coastlines (white outlines) on continents (gray) are shown. Mollweide projection.

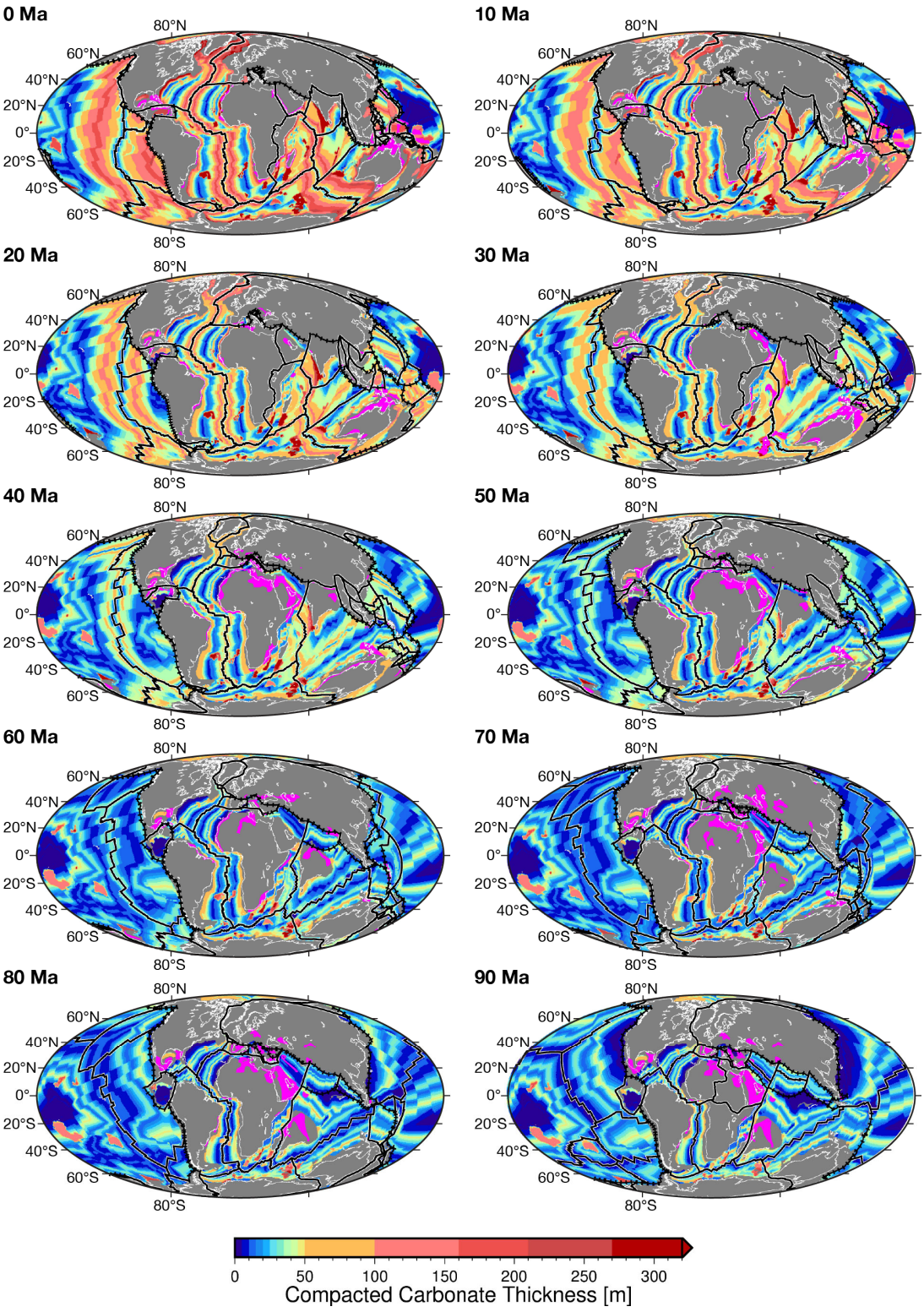

Figure DR3. Modelled compacted deep-sea carbonate thickness shown at 10 Myr intervals. Subduction zones (black hatched lines), other plate boundaries (black lines with white outlines), carbonate platforms from Kiessling et al. (2003) (magenta), and paleo-coastlines (white outlines) on continents (gray) are shown. Mollweide projection.

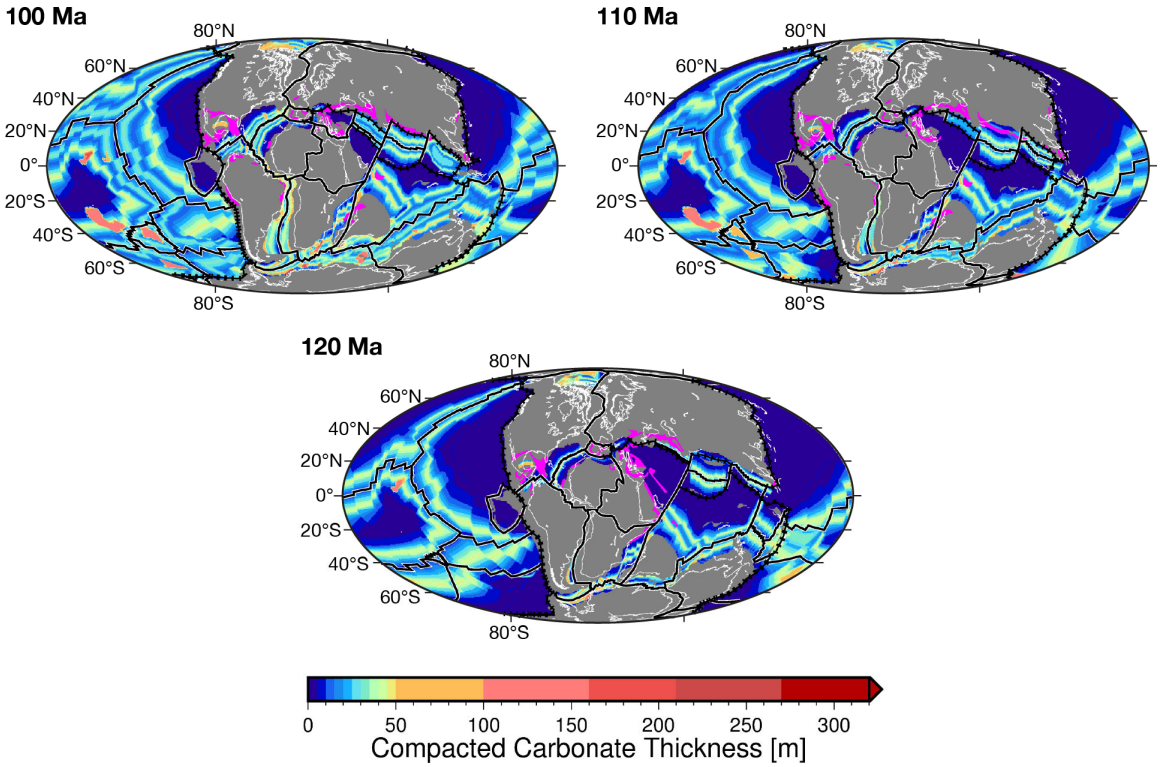

Figure DR3 cont. Modelled compacted deep-sea carbonate thickness shown at 10 Myr intervals. Subduction zones (black hatched lines), other plate boundaries (black lines with white outlines), carbonate platforms from Kiessling et al. (2003) (magenta), and paleo-coastlines (white outlines) on continents (gray) are shown. Mollweide projection.

REFERENCES

Amante, C., and Eakins, B. W., 2009, ETOPO1 1 Arc-Minute Global Relief Model: Procedures, Data Sources and Analysis, National Geophysical Data Center, NOAA, NOAA Technical Memorandum NESDIS NGDC-24, NOAA Technical Memorandum NESDIS NGDC-24.

Baumann, K.-H., Andruleit, H., Böckel, B., Geisen, M., and Kinkel, H., 2005, The significance of extant coccolithophores as indicators of ocean water masses, surface water temperature, and palaeoproductivity: a review: Paläontol. Z., v. 79, no. 1, p. 93-112.

Berger, W. H., 2011, Geologist at sea: aspects of ocean history: Annu. Rev. Earth Planet. Sci., v. 3, p. 1-34.

Bornemann, A., Aschwer, U., and Mutterlose, J., 2003, The impact of calcareous nannofossils on the pelagic carbonate accumulation across the Jurassic–Cretaceous boundary: Palaeogeog. Palaeoclim. Palaeoecol., v. 199, no. 3, p. 187-228.

Boss, S. K., and Wilkinson, B. H., 1991, Planktogenic/eustatic control on cratonic/oceanic carbonate accumulation: The Journal of Geology, v. 99, no. 4, p. 497-513.
Bown, P. R., Lees, J. A., and Young, J. R., 2004, Calcareous nannoplankton evolution and diversity through time, *in* Thierstein, H. R., and Young, J. R., eds., Coccolithophores—From Molecular Processes to Global Impact: Berlin, Springer, p. 481-508.
Broecker, W. S., and Peng, T. H., 1982, Tracers in the Sea, Palisades, New York, Eldigio Press, 690 p.:
Davies, T. A., and Worsley, T. R., 1981, Paleoenvironmental implications of oceanic carbonate sedimentation rates: SEPM Spec. Pub. No. 32, p. 169-179.
Dutkiewicz, A., Müller, R. D., Wang, X., O'Callaghan, S., Cannon, J., and Wright, N. M., 2017, Predicting sediment thickness on vanished ocean crust since 200 Ma: Geochemistry, Geophysics, Geosystems, v. 18, no. 12, p. 4586-4603.
Hay, W. W., 2004, Carbonate fluxes and calcareous nannoplankton, *in* Thierstein, H. R., and Young, J. R., eds., Coccolithophores—From Molecular Processes to Global Impact: Berlin, Springer, p. 509-528.
Kennett, J. P., 1982, Marine Geology, Prentice Hall, Englewood Cliffs, NJ, 813 p.:
Kiessling, W., Flügel, E., and Golonka, J., 2003, Patterns of Phanerozoic carbonate platform sedimentation: Lethaia, v. 36, no. 3, p. 195-225.
Knoll, A. H., 2003, Biomineralization and evolutionary history: Rev. Mineral. Geochem., v. 54, no. 1, p. 329-356.
Kominz, M. A., Patterson, K., and Odette, D., 2011, Lithology dependence of porosity in slope and deep marine sediments: J. Sed. Res., v. 81, no. 10, p. 730-742.
Milliman, J. D., 1993, Production and accumulation of calcium carbonate in the ocean: budget of a nonsteady state: Global Biogeochemical Cycles, v. 7, no. 4, p. 927-957.
Müller, R. D., and Dutkiewicz, A., 2018, Oceanic crustal carbon cycle drives 26 million-year atmospheric carbon dioxide periodicities: Science Advances, v. 4, p. eaaq0500.
Müller, R. D., Sdrolias, M., Gaina, C., Steinberger, B., and Heine, C., 2008, Long-term sea level fluctuations driven by ocean basin dynamics: Science, v. 319, no. 5868, p. 1357-1362.
Müller, R. D., Seton, M., Zahirovic, S., Williams, S. E., Matthews, K. J., Wright, N. M., Shephard, G. E., Maloney, K., Barnett-Moore, N., Hosseinpour, M., Bower, D. J., and Cannon, J., 2016, Ocean basin evolution and global-scale plate reorganization events since Pangea breakup: Annual Review of Earth and Planetary Science, v. 44, p. 107-138.
Opdyke, B. N., and Wilkinson, B. H., 1988, Surface area control of shallow cratonic to deep marine carbonate accumulation: Paleoceanography, v. 3, no. 6, p. 685-703.
Ridgwell, A., and Zeebe, R. E., 2005, The role of the global carbonate cycle in the regulation and evolution of the Earth system: Earth and Planetary Science Letters, v. 234, no. 3, p. 299-315.
Roth, P. H., 1986, Mesozoic palaeoceanography of the North Atlantic and Tethys oceans, *in* Summerhayes, C. P., and Shackleton, N. J., eds., North Atlantic

Palaeoceanography, Geological Society, London, Spec. Pub. No. 21: Oxford, UK, Blackwell, p. 299-320.
-, 1989, Ocean circulation and calcareous nannoplankton evolution during the Jurassic and Cretaceous: Paleogeog. Paleoclim. Paleoecol., v. 74, no. 1-2, p. 111-126.
Stein, C. A., and Stein, S., 1992, A model for the global variation in oceanic depth and heat flow with lithospheric age: Nature, v. 359, no. 6391, p. 123-129.
Van Andel, T. H., 1975, Mesozoic/Cenozoic calcite compensation depth and the global distribution of calcareous sediments: Earth Planet. Sci. Lett., v. 26, no. 2, p. 187-194.
Whitman, J. M., and Davies, T. A., 1979, Cenozoic oceanic sedimentation rates: how good are the data?: Mar. Geol., v. 30, no. 3-4, p. 269-284.